2018 21st International Conference on Intelligent Transportation Systems (ITSC)
Maui, Hawaii, USA, November 4-7, 2018

Comparison of Feedback Linearization and Model Predictive Techniques for Variable Speed Limit Control

Yihang Zhang[1], Isik Ilber Sirmatel[2], Faisal Alasiri[1], Petros A. Ioannou[1] and Nikolas Geroliminis[2]

Abstract— **Different types of variable speed limit (VSL) controllers have been proposed to improve the traffic mobility at highway bottlenecks. However, the benefit of VSL is sometimes deteriorated by the capacity drop phenomenon introduced by the disordered lane changes at the vicinity of the bottleneck. Our recent results show that by combining the VSL controller with lane change control, the capacity drop can be significantly relieved or avoided at the bottleneck. In this paper, we propose feedback linearization and model predictive control schemes for VSL-actuated highway traffic, where a lane change controller is assumed to be active upstream of the bottleneck. Via simulation studies, we compare the performance and robustness of the proposed controllers with respect to perturbations on traffic demand, model parameters and measurement noise. Results show that both controllers are able to improve the total time spent under different levels of perturbation and noise. Furthermore, feedback linearization VSL can provide better performance than model predictive VSL with negligible computational effort and similar robustness.**

I. Introduction

Due to the rapidly increasing demand for transportation and mobility, managing the highway traffic flow with intelligent transportation technologies has become vital to improve the efficiency of the existing highway infrastructure, thus avoid or relieve highway congestion and improve the traffic mobility, safety and environmental impact. Variable speed limit (VSL) control is one of the most commonly used and studied control techniques designed to regulate the traffic flow on highways. Previous studies have demonstrated that by adjusting the speed limit upstream the highway bottleneck, VSL is able to improve mobility in the highway [1]–[10]. A number of VSL control strategies are proposed in previous literatures, which can be classified as follows:

1. *Feedback control based VSL.* Feedback VSL controller generates the VSL commands based on current and previous traffic states. In 2013, Carlson et al. proposed a local feedback controller and demonstrated that the simple feedback controller can provide improvement with respect to the total time spent (TTS) similar to the optimal control strategy albeit using much lower computational effort [1]. The method is extended to multiple bottlenecks in [2] and combined with upstream delay balance in [11]. In [3], Jin and Jin proposed a proportional-integral (PI) VSL controller to maximize the bottleneck throughput with one VSL sign upstream the bottleneck by locally stabilizing the vehicle density at a critical value. In [4], Zhang and Ioannou combined lane change (LC) control with a feedback linearization (FL) VSL controller which guarantees global exponential stability.

2. *Model predictive control (MPC) based VSL.* MPC based VSL control strategies compute the VSL commands by predicting the system behavior with dynamic models and solving finite-horizon optimal control problems at each time step in a receding horizon manner. Muralidharan et al. proposed a MPC VSL controller based on the link-node cell transmission model that can recover the bottleneck from capacity drop and obtain an optimal trajectory in the absence of capacity drop [5]. In [7], an MPC-based VSL controller was proposed to improve traffic safety, mobility and the environmental impact simultaneously in a connected vehicle context. In [12], a MPC method is proposed based on a discrete first order model which takes into consideration the jam wave propagation. In general, MPC does not guarantee stability of the closed-loop system. Although some modified MPC approaches are able to stablize the system [13], it is still difficult to find a stablizing MPC controller for the VSL control problems due to the nonlinearity of the system and the non-convexity of the optimization problem.

3. *Optimal control based VSL.* Optimal control based VSL control strategies generate the VSL commands by solving an optimal control problem over the entire simulation time span and apply this pre-decided VSL command sequence to the system in an open-loop manner. In contrast to the real-time optimizations in MPC-VSL, optimal control based VSL solves the optimal control problem only once in an offline manner and does not consider the actual evolution of the states in real-time, which may be adversely affected by model uncertainty, disturbances, and measurement noise. An optimal control framework for highway network flow is proposed in [8], whereas [1] applied the framework on VSL controller design to minimize the TTS. In 2016, Como et al. showed the convexity of the optimal VSL control problem with a TTS cost function based on the cell transmission model (CTM) [9].

4. *Shockwave theory based VSL.* Shockwave theory based VSL strategies model the traffic flows as kinematic waves and use speed limit to control the propagation of the waves. In [10], Hegyi et al. proposed the SPECIALIST VSL control strategy based on shockwave theory, which detects the shockwave upstream the bottleneck and uses VSL to make

*This work has been supported by the METRANS Transportation Center under the following grants: Pacific Southwest Region 9 University Transportation Center (USDOT or Caltrans), National Center for Sustainable Transportation (USDOT or Caltrans) and Metrofreight

[1]Yihang Zhang, Faisal Alasiri and Petros A. Ioannou are with the Department of Electrical Engineering, University of Southern California, Los Angeles, 90045 {yihangzh, alasiri, ioannou}@usc.edu

[2]Isik Ilber Sirmatel and Nikolas Geroliminis are with the School of Architecture, Civil and Environmental Engineering École Polytechnique Fédérale de Lausanne (EPFL), 1015 Lausanne, Switzerland {isik.sirmatel, nikolas.geroliminis}@epfl.ch

the shockwave accumulate slower and dissipate faster, thus dampening the shockwave and improving mobility.

Although most of the above works on VSL claim significant improvement on traffic mobility, there are also a number of studies questioning the reported improvements on travel time under different incident scenarios, [14]–[17]. [4] demonstrated that the inconsistency between analysis and microscopic simulations is mainly caused by the capacity drop phenomenon, one of the major reasons of which is the forced lane changes in the vicinity of the bottleneck. This decreases the speed of vehicles in neighboring lanes, making it difficult, if not impossible, for VSL to eliminate congestion. [4] shows that by providing lane change recommendations to vehicles upstream of the bottleneck, it is possible to make most of the lane changes happen away from the incident. Thus, the capacity drop is dramatically reduced, based on which a FL VSL controller is designed in order to guarantee global exponential stability of the desired equilibrium point at which the maximum bottleneck flow is achieved.

Given the fact that LC control is able to relieve or avoid the capacity drop, one important question arises here is that if other VSL control strategies are combined with the LC control, will the system performance exceed the performance under the FL controller? Intuitively, since MPC control follows an optimization based routine, it should provide the 'optimal' performance to some extent. However, FL controller guarantees exponential stability of the equilibrium point with highest bottleneck flow rate. Therefore, by tuning the feedback gain, the FL controller should be able to force the system to converge as fast as possible, only limited by the saturation of control input.

In this paper, we propose FL and MPC schemes for VSL-actuated highway traffic, where we assume that an LC controller is active for the bottleneck. Both controllers are designed with a CTM-based model representing the ideal system. TTS performance and robustness with respect to perturbations on model parameters and measurement noise of the proposed controllers are evaluated via simulation studies. Results show both VSL controller is able to improve the total time spent under different levels of perturbation and measurement noise. Furthermore, feedback linearization VSL can provide better performance than model predictive VSL with much less computational effort.

The rest of this paper is organized as follows: In section II, cell transmission model of highway traffic and the effects of LC and VSL controller on the bottleneck model are studied. Section III provides details on the design of FL and nonlinear MPC (NMPC) schemes for VSL-actuated highway traffic. Simulation results are illustrated in section IV, where the performance and robustness of the FL and MPC schemes are compared. Section V concludes the paper.

II. System Modeling

A. Bottleneck Model

A highway segment consisting of 3 lanes is illustrated in Fig. 1. An incident blocking the middle lane is introduced

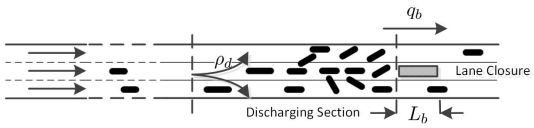

Fig. 1: Highway Bottleneck

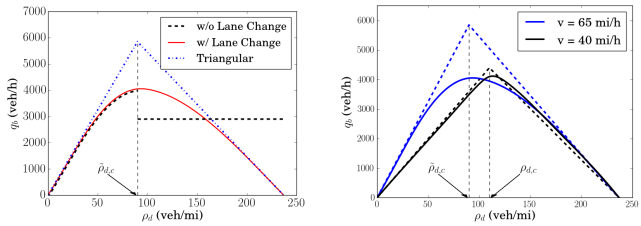

(a) w/ and w/o LC (b) w/ and w/o VSL

Fig. 2: Effects of LC and VSL on Fundamental Diagrams

thus forms a bottleneck. L_b denotes the length of the bottleneck, which is assumed to be small so that the effect of the density within L_b is negligible to affect the bottleneck flow. The speed limit upstream the bottleneck is fixed to the free flow speed, which is $v_f = 65$ mi/h. The black dashed line in Fig. 2a shows the relation between the vehicle density in the discharging section ρ_d and the bottleneck flow q_b. As can be noticed from Fig. 2a, when ρ_d is less than the critical value $\tilde{\rho}_{\mathrm{d,c}}$, the value of q_b increases with ρ_d. However, when ρ_d exceeds the critical value $\tilde{\rho}_{\mathrm{d,c}}$, a queue will form at the bottleneck since the demand of the bottleneck is higher than its capacity. Consequently, the speed of traffic will decrease because of the lane changes undertaken by vehicles in the queue. Therefore, the flow rate will also drop to be lower than the bottleneck capacity. This capacity drop phenomenon makes it difficult for VSL controllers to increase the value of q_b at the bottleneck since VSL only regulates the average density ρ_d in the discharging section and cannot do anything related to the lane changes at the vicinity of the bottleneck.

Allowing drivers to proactively alter their lanes by providing appropriate recommendations leads to relief or avoidance of the capacity drop [4]. As shown by the red solid line in Fig. 2a, the fundamental diagram becomes continuous at the critical density. Applying the LC control makes it possible for the VSL to stabilize ρ_d at $\tilde{\rho}_{d,c}$, where the maximum possible q_b is achieved. Looking more closely at the fundamental diagram with LC control, it can be noticed that it is very close to its triangular approximation when the value of ρ_d is small, meaning that the flow speed is close to the free flow speed, and the flow speed decreases as ρ_d approaches $\tilde{\rho}_{d,c}$. [4] concluded that the speed reduction is due to modeling error, delay in following the speed limits, and drivers behavior when passing by an incident zone. The reduction in speed will not harm the benefit of VSL controller in bottleneck flow as long as ρ_d is stabilized at $\tilde{\rho}_{\mathrm{d,c}}$. However, if the speed limit of the upstream segment of the bottleneck is v_f, drivers need to accelerate and then decelerate when approaching the bottleneck, resulting in shockwaves that

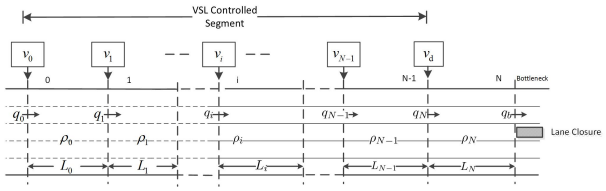

Fig. 3: Configuration of the Highway Segment

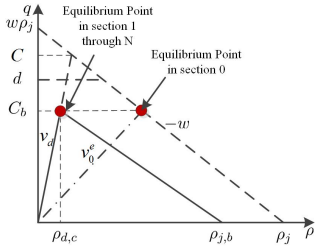

Fig. 4: Desired Equilibrium Point

propagate upstream. Decreasing the upstream speed limit of the bottleneck to v_d, such that $0 < v_d < v_f$, shifts the critical density in the fundamental diagram to a higher value and decreases the slope of the under-critical part, and it would be close to a straight line [4], [18]. The black solid line in Fig. 2b depicts the fundamental diagram using a speed limit of 40 mi/h, which shows that the capacity of the bottleneck does not decrease together with the upstream speed limit, as the critical density increases from $\tilde{\rho}_{\mathrm{d,c}}$ to $\rho_{\mathrm{d,c}}$. Here the fundamental diagram is very close to its triangular approximation and the deviation of the speed is very small at $\rho_d = \rho_{d,c}$. By enforcing the VSL command to converge to v_d at the equilibrium state, the shockwave upstream of the bottleneck will be attenuated. Under the speed limit of v_d and the assumption of triangular fundamental diagram, the model of highway bottleneck is as follows:

$$q_{\mathrm{b}} = \begin{cases} v_{\mathrm{d}}\rho_d, & \rho_d \le \rho_{\mathrm{d,c}} \\ w_{\mathrm{b}}(\rho_{\mathrm{j,d}} - \rho_d), & \rho_d > \rho_{\mathrm{d,c}}, \end{cases} \tag{1}$$

where $\rho_{\mathrm{j,d}} = v_{\mathrm{d}}\rho_{d,c}/w_{\mathrm{b}} + \rho_{d,c}$.

B. Cell Transmission Model

As can be seen in Fig. 3, the upstream highway segment of the bottleneck is divided into $N+1$ sections, which are not necessarily identical in length. VSL signs are placed at the beginning of section 0 through section $N-1$. Closure of a lane in section N introduces the bottleneck. ρ_i , v_i, and q_i are the vehicle density, VSL command, and in-flow rate in section i, respectively, where $i = 0, 1, , N-1$. In section N, the speed limit is constant, denoted by v_d. The flow rate through the bottleneck is represented by q_b. By the conservation law, the differential equations that describe the dynamics of the densities are as follows:

$$\begin{aligned} \dot{\rho_i} &= \frac{1}{L_i}(q_i - q_{i+1}), \quad \text{for } i = 0, 1, ..., N-1 \\ \dot{\rho_N} &= \frac{1}{L_N}(q_N - q_b). \end{aligned} \tag{2}$$

Under the assumption of triangular fundamental diagram, we have

$$\begin{aligned} q_0 &= \min\{d, C_0, w_0(\rho_{\mathrm{j},0} - \rho_0)\} \\ q_i &= \min\{v_{i-1}\rho_{i-1}, C_i, w_i(\rho_{\mathrm{j},i} - \rho_i)\}, i = 1, \ldots, N, \end{aligned} \tag{3}$$

where d is the demand flow of this highway segment. Here we assume $d > C_b$ is constant. $\rho_{\mathrm{j},i}$ is the jam density of section i, at which q_i would be 0. w_i is the backward propagating wave speed in section i. C_i is the capacity, i.e. the maximum possible flow rate in section i, given by $C_i = v_i w_i \rho_{\mathrm{j},i}/(v_i + w_i)$. L_i is the length of section i.

In Fig. 3, section N is the discharging section. By applying the LC control in section N, capacity drop at the bottleneck can be removed. According to (1), we have

$$q_{\mathrm{b}} = \begin{cases} v_{\mathrm{d}}\rho_N, & \rho_N \le \rho_{\mathrm{d,c}} \\ w_{\mathrm{b}}(\rho_{\mathrm{j,d}} - \rho_N), & \rho_N > \rho_{\mathrm{d,c}} \end{cases} \tag{4}$$

and the capacity of the bottleneck is $C_b = v_d\rho_{\mathrm{d,c}}$.

In order to track the number of vehicles that accumulate upstream of section 0, we introduce a new state Q, that is

$$\dot{Q} = d - q_0, \tag{5}$$

with $Q = 0$ at $t = 0$. Therefore, if the number of vehicles upstream of section 0 is greater than the number at time 0, $Q > 0$, otherwise $Q \le 0$. We should note here that the introduction of Q is only for the purpose of evaluating the TTS. It demonstrates the part of upstream demand which cannot enter section 0, based on the equations (2) - (4). Both the FL and MPC controllers are implemented based on system (2) - (4). The performance metric TTS is defined as follows:

$$\mathrm{TTS} = \int_0^T \left(Q(t) + \sum_{i=0}^{N} \rho_i(t) L_i \right) dt \tag{6}$$

III. Control Design

A. Desired Equilibrium Point

As discussed in Section II-A, we select v_d such that $0 < v_d < v_f$ to be the equilibrium speed limit in order to reduce the speed deviation. In Fig. 4, the fundamental diagram of the bottleneck section is the solid line and the fundamental diagram of the non-bottleneck sections is the dashed line. Considering both the mobility of the network and homogeneity of the traffic flow, we set the equilibrium point to be

$$\begin{aligned} &\rho_i^e = \rho_{\mathrm{d,c}}, \ v_i^e = v_d, \ \text{for } i = 1, \ldots, N. \\ &\rho_0^e = \rho_{j,0} - C_b/w_0, v_0^e = C_b/\rho_0^e \end{aligned} \tag{7}$$

As shown in Fig. 4, at the equilibrium point (7), inflow and outflow of each section are the same and equal the bottleneck capacity C_b. Around the equilibrium point (7), the system (2) - (4) can be expressed as follows:

$$\begin{aligned} \dot{\rho}_0 &= (w_0(\rho_{\mathrm{j},0} - \rho_0) - v_0\rho_0)/L_0 \\ \dot{\rho}_i &= (v_{i-1}\rho_{i-1} - v_i\rho_i, \ \text{for }\,)/L_i, \quad i = 1, \ldots, N-1 \\ \dot{\rho}_N &= \begin{cases} (v_{N-1}\rho_{N-1} - v_{\mathrm{d}}\rho_N)/L_N, & \rho_N \le \rho_{\mathrm{d,c}} \\ (v_{N-1}\rho_{N-1} - w_{\mathrm{b}}(\rho_{\mathrm{j,b}} - \rho_N))/L_N, & \rho_N > \rho_{\mathrm{d,c}} \end{cases} \end{aligned} \tag{8}$$

We define the error system as: $e_i = \rho_i - \rho_i^{\mathrm{e}}$ for $i = 0, 2, , \ldots, N$ and $u_i = v_i - v_i^{\mathrm{e}}$ for $i = 0, 1, \ldots, N-1$. Substituting into (8), we have

$$\begin{aligned}
\dot{e}_0 &= (-w_0 e_0 - v_0^{\mathrm{e}} e_0 - u_0 \rho_0)/L_0 \\
\dot{e}_i &= (v_{i-1}^{\mathrm{e}} e_{i-1} + u_{i-1}\rho_{i-1} - v_i^{\mathrm{e}} e_i - u_i \rho_i)/L_i \\
&\qquad\qquad \text{for } i = 1, \ldots, N-1 \\
\dot{e}_N &= \begin{cases} (v_{N-1}^{\mathrm{e}} e_{N-1} + u_{N-1}\rho_{N-1} - v_{\mathrm{d}} e_N)/L_N, & e_N \le 0 \\ (v_{N-1}^{\mathrm{e}} e_{N-1} + u_{N-1}\rho_{N-1} + w_{\mathrm{b}} e_N)/L_N, & e_N > 0 \end{cases}
\end{aligned} \tag{9}$$

The transformation of (8) to (9) shifts the nonzero equilibrium state of (8) to the zero equilibrium point of (9). Letting $e = [e_0, e_1, ..., e_N]^T$, and $u = [u_0, u_1, ..., u_{N-1}]^T$, we can implicitly express system (9) as:

$$\dot{e} = f(e, u) \tag{10}$$

B. Feedback Linearization Controller

According to [4], we design the FL-VSL controller based on system (9) as follows:

$$\begin{aligned}
u_i &= (-v_i^{\mathrm{e}} e_i - \lambda_i L_i e_{i+1})/\rho_i, \text{ for } i = 0, \ldots, N-2 \\
u_{N-1} &= \begin{cases} \dfrac{-\lambda_{N-1} L_N e_N - v_{N-1}^{\mathrm{e}} e_{N-1} + v_{\mathrm{d}} e_N}{\rho_{N-1}}, & e_N \le 0 \\ \dfrac{-\lambda_{N-1} L_N e_N - v_{N-1}^{\mathrm{e}} e_{N-1} - w_{\mathrm{b}} e_N}{\rho_{N-1}}, & e_N > 0 \end{cases}
\end{aligned} \tag{11}$$

where $\lambda_i > 0$ for $i = 0, \ldots, N-1$ are design parameters. With the FL controller (11), the closed-loop system becomes:

$$\begin{aligned}
\dot{e}_0 &= -\frac{w_0}{L_0} e_0 + \lambda_0 e_1 \\
\dot{e}_i &= -\lambda_{i-1}\frac{L_{i-1}}{L_i} e_i + \lambda_i e_{i+1}, \text{for } i = 1 \ldots, N-2 \\
\dot{e}_{N-1} &= \begin{cases} -\lambda_{N-2}\frac{L_{N-1}}{L_{N-1}} e_{N-1} + (\lambda_{N-1} - \frac{v_d}{L_{N-1}}) e_N, & e_N \le 0 \\ -\lambda_{N-2}\frac{L_{N-1}}{L_{N-1}} e_{N-1} + (\lambda_{N-1} + \frac{w_b}{L_{N-1}}) e_N, & e_N > 0 \end{cases} \\
\dot{e}_N &= -\lambda_{N-1}\frac{L_{N-1}}{L_N} e_N
\end{aligned} \tag{12}$$

Theorem 1 in [4] shows that with the FL controller (11), the zero equilibrium point of the closed-loop system (12) is guaranteed to be globally exponentially stable.

Considering safety and driver acceptance in the real world, we keep the VSL commands constant within the time interval $(kT_c, (k+1)T_c]$, where $k = 0, 1, 2, ...$ and T_c is the control step size. The following constraints are also applied to the VSL command. Let $u_i(k)$ denotes u_i computed by equation (11) at $t = kT_{\mathrm{c}}$. We have,

$$\bar{v}_i(k) = [v_i^{\mathrm{e}} + u_i(k)]_5 \tag{13}$$

$$\tilde{v}_i(k) = \max\{\bar{v}_i(k), v_i(k-1) - C_{\mathrm{v}}, v_{i-1}(k) - C_{\mathrm{v}}\} \tag{14}$$

$$v_i(k) = \begin{cases} v_{\max}, & \text{if } \tilde{v}_i(k) > v_{\max} \\ v_{\min}, & \text{if } \tilde{v}_i(k) < v_{\min} \\ \tilde{v}_i(k), & \text{otherwise} \end{cases} \tag{15}$$

for $i = 0, 2, \ldots, N-1, k = 0, 1, 2, \ldots$.

In (13), $[\cdot]_5$ is the operator which rounds a real number to its closest multiple of 5. Equation (14) describes the saturation on the amount of decrease of VSL commands between successive control steps and highway sections, C_v is the maximum decrease allowed. In (15), $v_{\max}$ and $v_{\min}$ are the upper and lower bounds of VSL commands, respectively.

C. Nonlinear Model Predictive Control

Here we formulate the problem of finding the VSL commands $u(\cdot)$ that try to maintain system (10) at the equilibrium point as the following finite-horizon constrained optimal control problem (OCP):

$$\begin{aligned}
\underset{u(\cdot)}{\text{minimize}} \quad & \int_{kT_c}^{kT_c+T_p} e(\tau)^T \tilde{Q} e(\tau) + u(\tau)^T \tilde{R} u(\tau) d\tau \\
\text{subject to} \quad & e(kT_c) = \hat{e}(kT_c) \\
& \forall \tau \in [t, t+T_p]: \\
& \quad \dot{e} = f(e, u) \\
& \quad v_{\min} - v_e \le u(\tau) \le v_{\max} - v_e,
\end{aligned} \tag{16}$$

where t is the current control sampling instant in time, $\hat{e}(t)$ is the measurement on error states taken at that instant, $\tilde{Q}$ and $\tilde{R}$ are weight matrices on error and control input, respectively, whereas T_p is the prediction horizon. The optimization problem is solved at the beginning of each control step kT_c, with $\hat{e}(kT_c)$ as the initial condition. Constraint (15) has already been included in the constraints of the optimization problem. (13) and (14) are also applied to the MPC VSL commands before applied to the system. Since the equality constraint of problem (16) is nonlinear, the optimization problem is non-convex [19].

Due to the continuous-time dynamics, the OCP (16) is an infinite dimensional optimization problem. We resort to approximating it as a finite dimensional nonlinear program (NLP) via the direct multiple shooting method [20]. Details on direct methods from numerical optimal control literature can be found in [21].

IV. Numerical Simulation

In this section, macroscopic simulation is used to evaluate the performance and robustness of the FL and MPC schemes combined with LC control.

A. Scenario setup

The proposed controllers are evaluated on a southbound segment on the I-710 freeway (between I-105 junction and the Long Beach Port), California, United States of America. The segment of the highway is divided into 8 sections where the VSL signs are placed at the beginning of section 0 through 6. In order to create a bottleneck, an incident that blocks the middle lane of a 3-lane segment is introduced at the end of section 7. The LC control is deployed at the beginning of section 7. The simulation network is calibrated with real world data from the PeMs system [22]. Without an incident, the capacity of the highway segment is 6800 veh/h. The ideal capacity of the bottleneck after the incident occurs is about 4500 veh/h. In our simulation, the incident happens

5 minutes after the simulation starts, and it lasts for 30 min. The nominal demand is 6000 veh/h. The desired equilibrium point of this network is calibrated to be:

$$\rho_0^{\mathrm{e}} = 278 \text{ veh/mi},\ \rho_1^{\mathrm{e}} = \rho_2^{\mathrm{e}} = \cdots = \rho_7^{\mathrm{e}} = 110 \text{ veh/mi}$$
$$v_0^{\mathrm{e}} = 15.8 \text{ mi/h},\ v_1^{\mathrm{e}} = v_2^{\mathrm{e}} = \cdots = v_7^{\mathrm{e}} = 40 \text{ mi/h}$$

For the FL controller, we choose $\lambda_i = 50$ for $i = 0, 1, \ldots, 6$. $C_v = 10$ mi/h, $v_{\min} = 10$ mi/h and $v_{\max} = 65$ mi/h. The MPC controller is implemented using the direct multiple shooting method via the CasADi toolbox [23] in MATLAB 8.5.0 (R2015a), on a 64-bit Windows PC with 3.4-GHz Intel Core i7 processor and 8-GB RAM, where IPOPT [24] is used for solving the NLPs. In our simulation, we choose the prediction horizon $T_p = 10$ min, which is much greater than the control time step $T_c = 30$ s. Weight matrices are chosen as $\tilde{Q} = \mathbf{I}$ and $\tilde{R} = 0.1\mathbf{I}$, with $\mathbf{I}$ denoting the identity matrix of appropriate dimensions. The feedback gain for FL and the prediction horizon T_p for MPC is tuned so that best performance in terms of total time spent is achieved for both controllers. Specifically for MPC, together with the increase of T_p, the closed-loop performance is improved but the computation time also increases. When $T_p \geq 10$ min, the closed loop performance will not improve with T_p. With $T_p = 10$ min, The computation time of MPC is around 0.35 seconds, whereas it is negligible for FL. The MPC scheme is still computationally tractable, as its computation time of 0.35 s per step is negligible with respect to the control time step of 30 s.

B. Performance and Robustness Analysis

To compare the performance and robustness of the FL and MPC VSL controllers, we evaluate the following criteria for the two controllers: 1) Total time spent (TTS) as defined in (6), and sensitivity of TTS with respect to 2) perturbation on traffic demand, 3) perturbation on model parameters and 4) measurement noise. In the simulation, the FL and MPC controllers are synthesized with the ideal model (10), but the control command are applied on a perturbed model. For the traffic demand, we add up to $\pm 20\%$ perturbation on the nominal demand 6000 veh/h. For the model parameters, as shown in Fig. 5, we respectively add up to $\pm 20\%$ perturbation on the nominal value of $\rho_{d,c}$ and C_b, which directly alter the shape of the fundamental diagram of the bottleneck section. For the measurement noise, we add Gaussin white noise to the measuement of vehicle densities as $\hat{\rho}_i = \rho_i + n_i$, where $\hat{\rho}_i$ is the measument of ρ_i, n_i is the Gaussian white noise. The standard deviation of the noise is up to $\sigma(n_i) = 0.1\rho_{d,c}$ to match the scale of the density measurements.

Fig. 6 shows the behavior of the vehicle density in the discharging section under FL and MPC controller. Both controllers are able to maintain the density around the desired value $\rho_7^e = 110$ veh/h after the incident occurs at $t = 5$ min. The oscillation is introduced by the roundup-to-5 constraint. However, the MPC controller introduces higher frequency chattering and a sharp decrease at the beginning of the incident.

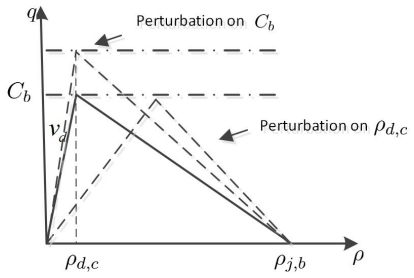

Fig. 5: Simulation System

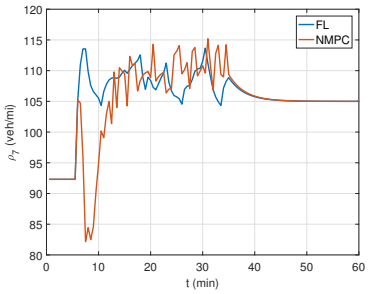

Fig. 6: ρ_7 with FL and MPC

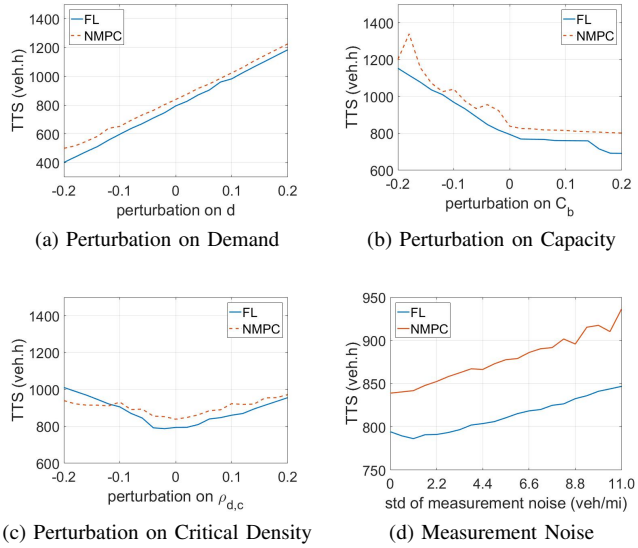

(a) Perturbation on Demand

(b) Perturbation on Capacity

(c) Perturbation on Critical Density

(d) Measurement Noise

Fig. 7: Performance Sensitivity of FL and MPC Controller

A series of simulation experiments are conducted with different levels of perturbation and measurement noise. Figure 7a shows how TTS varies with varying demand levels. The figure showcases that both controllers are able to function properly under various levels of demand, the TTS increases and decreases approximately linear with the demand. This demonstrates that both MPC and FL VSL controllers are robust with respect to the variation of demand, which is due to the selection of the desired equilibrium point (7). At the equilibrium point, the speed limit in section 0 is decreased to block excessive traffic demand upstream of the entire control segment, therefore the bottleneck flow is not

affected. Furthermore, under different levels of perturbation, the performance of FL and MPC controller are similar. But the TTS of FL is always slightly lower than that of MPC, which shows that MPC fails to beat FL in TTS although the control commands are generated by solving the optimization problem in receding horizon fashion.

In figures 7b and 7c, the change in TTS is plotted with respect to different values of perturbation on C_b and $\rho_{\mathrm{d,c}}$, respectively. These results show that both controllers achieve significant improvements over the no control case and are able to operate properly even under situations with high level of uncertainty in these model parameters. With perturbation on C_b, the TTS under FL and MPC are increased by 45% and 43% in the worst case, respectively. Considering the fact that in this case the bottleneck capacity is decreased by 20% as a baseline, the TTS does not increase too much due to the modeling error. The worst case for the perturbation on $\rho_{\mathrm{d,c}}$ is 27% worse than the non-perturbed value for FL, and 16% for MPC.

The sensitivity of TTS performance in the case of varying levels of standard deviation in measurement noise is given in figure 7d, which shows that the TTS under both controllers increases with the standard deviation of measurement noise. However, the system does not diverge as the no control case. The performance of FL is always better than that of MPC in this case.

Although the MPC controller is built based on an optimization scheme, it only achieves optimality over each prediction horizon instead of the entire control period. Furthermore, the FL controller guarantees global exponential convergence, which is the best possible performance from the control point of view, while the MPC controller achieved from (16) does not guarantee stability of the equilibrium point. Therefore, the MPC controller fails to achieve better performance comparing to the FL controller.

V. Conclusion

In this paper, we combined the feedback linearization and model predictive VSL controllers with the LC controller, respectively. With total time spent as performance criterion, we evaluated and compared the performance and robustness with respect to perturbation on traffic demand, model parameters and measurement noise of the two controllers. Simulation results show that both controllers work properly under different levels of perturbation and measurement noise. Although the synthesis of MPC controller involves an optimal control routine and is computationally much more expensive, it does not provide better performance than the feedback linearization.

References

[1] R. C. Carlson, I. Papamichail, and M. Papageorgiou, "Comparison of local feedback controllers for the mainstream traffic flow on freeways using variable speed limits," *Journal of Intelligent Transportation Systems*, vol. 17, no. 4, pp. 268–281, 2013.

[2] G.-R. Iordanidou, C. Roncoli, I. Papamichail, and M. Papageorgiou, "Feedback-based mainstream traffic flow control for multiple bottlenecks on motorways," *IEEE Transactions on Intelligent Transportation Systems*, vol. 16, no. 2, pp. 610–621, 2015.

[3] H.-Y. Jin and W.-L. Jin, "Control of a lane-drop bottleneck through variable speed limits," *Transportation Research Part C: Emerging Technologies*, vol. 58, pp. 568–584, 2015.

[4] Y. Zhang and P. A. Ioannou, "Combined variable speed limit and lane change control for highway traffic," *IEEE Transactions on Intelligent Transportation Systems*, 2016.

[5] A. Muralidharan and R. Horowitz, "Computationally efficient model predictive control of freeway networks," *Transportation Research Part C: Emerging Technologies*, vol. 58, pp. 532–553, 2015.

[6] J. R. D. Frejo, A. Núñez, B. De Schutter, and E. F. Camacho, "Hybrid model predictive control for freeway traffic using discrete speed limit signals," *Transportation Research Part C: Emerging Technologies*, vol. 46, pp. 309–325, 2014.

[7] B. Khondaker and L. Kattan, "Variable speed limit: A microscopic analysis in a connected vehicle environment," *Transportation Research Part C: Emerging Technologies*, vol. 58, pp. 146–159, 2015.

[8] A. Kotsialos, M. Papageorgiou, M. Mangeas, and H. Haj-Salem, "Coordinated and integrated control of motorway networks via nonlinear optimal control," *Transportation Research Part C: Emerging Technologies*, vol. 10, no. 1, pp. 65–84, 2002.

[9] G. Como, E. Lovisari, and K. Savla, "Convexity and robustness of dynamic traffic assignment and freeway network control," *Transportation Research Part B: Methodological*, vol. 91, pp. 446–465, 2016.

[10] A. Hegyi, S. Hoogendoorn, M. Schreuder, H. Stoelhorst, and F. Viti, "Specialist: A dynamic speed limit control algorithm based on shock wave theory," in *2008 11th International IEEE Conference on Intelligent Transportation Systems*. IEEE, 2008, pp. 827–832.

[11] G. R. Iordanidou, I. Papamichail, C. Roncoli, and M. Papageorgiou, "Feedback-based integrated motorway traffic flow control with delay balancing," *IEEE Transactions on Intelligent Transportation Systems*, vol. PP, no. 99, pp. 1–11, 2017.

[12] Y. Han, A. Hegyi, Y. Yuan, S. Hoogendoorn, M. Papageorgiou, and C. Roncoli, "Resolving freeway jam waves by discrete first-order model-based predictive control of variable speed limits," *Transportation Research Part C: Emerging Technologies*, vol. 77, pp. 405 – 420, 2017.

[13] D. Q. Mayne, J. B. Rawlings, C. V. Rao, and P. O. Scokaert, "Constrained model predictive control: Stability and optimality," *Automatica*, vol. 36, no. 6, pp. 789–814, 2000.

[14] J. M. Torne Santos, D. Rosas, and F. Soriguera, "Evaluation of speed limit management on c-32 highway access to Barcelona," in *Transportation Research Board 90th Annual Meeting*, no. 11-2397, 2011.

[15] K. Gao, "Multi-objective traffic management for livability," Ph.D. dissertation, MS thesis, TU Delft, Delft, The Netherlands, 2012.

[16] L. Kejun, Y. Meiping, Z. Jianlong, and Y. Xiaoguang, "Model predictive control for variable speed limit in freeway work zone," in *2008 27th Chinese Control Conference*. IEEE, 2008, pp. 488–493.

[17] P. Ioannou, Y. Wang, A. Abadi, and V. Butakov, "Dynamic variable speed limit control: Design, analysis and benefits," Tech. Rep., 2012.

[18] M. Papageorgiou, E. Kosmatopoulos, and I. Papamichail, "Effects of variable speed limits on motorway traffic flow," *Transportation Research Record: Journal of the Transportation Research Board*, no. 2047, pp. 37–48, 2008.

[19] S. Boyd and L. Vandenberghe, *Convex optimization*. Cambridge university press, 2004.

[20] H. G. Bock and K.-J. Plitt, "A multiple shooting algorithm for direct solution of optimal control problems," in *Proceedings of the IFAC World Congress*, 1984.

[21] M. Diehl, H. G. Bock, H. Diedam, and P.-B. Wieber, "Fast direct multiple shooting algorithms for optimal robot control," in *Fast motions in biomechanics and robotics*. Springer, 2006, pp. 65–93.

[22] C. D. of Transportation. (2015) Caltrans performance measurement system (PeMS). [Online]. Available: http://pems.dot.ca.gov/

[23] J. Andersson, "A General-Purpose Software Framework for Dynamic Optimization," PhD thesis, Arenberg Doctoral School, KU Leuven, Department of Electrical Engineering (ESAT/SCD) and Optimization in Engineering Center, Kasteelpark Arenberg 10, 3001-Heverlee, Belgium, October 2013.

[24] A. Wächter and L. T. Biegler, "On the implementation of an interior-point filter line-search algorithm for large-scale nonlinear programming," *Mathematical Programming*, vol. 106, no. 1, pp. 25–57, 2006.